

Video Article

Structural Design and Manufacturing of a Cruiser Class Solar Vehicle

Giangiaco Minak^{1,2,3}, Tommaso M. Brugo¹, Cristiano Fragassa^{1,2}, Ana Pavlovic², Felipe V. de Camargo², Nicola Zavatta³

¹Department of Industrial Engineering, Università di Bologna

²CIRI MAM, Università di Bologna

³CIRI AERO, Università di Bologna

Correspondence to: Giangiacomo Minak at giangiaco.minak@unibo.it

URL: <https://www.jove.com/video/58525>

DOI: [doi:10.3791/58525](https://doi.org/10.3791/58525)

Keywords: Engineering, Issue 143, Carbon fiber, composite materials, ply-book, leaf spring, crash test, monocoque chassis, finite element analysis, experimental testing

Date Published: 1/30/2019

Citation: Minak, G., Brugo, T.M., Fragassa, C., Pavlovic, A., de Camargo, F.V., Zavatta, N. Structural Design and Manufacturing of a Cruiser Class Solar Vehicle. *J. Vis. Exp.* (143), e58525, doi:10.3791/58525 (2019).

Abstract

Cruisers are multi-occupant solar vehicles that are conceived to compete in long-range (over 3,000 km) solar races based on the best compromise between the energy consumption and the payload. They must comply to the race's rules regarding the overall dimensions, the solar panel size, functionality, and safety and structural requirements, while the shape, the materials, the powertrain, and the mechanics are considered at the discretion of the designer. In this work, the most relevant aspects of the structural design process of a full-carbon fiber-reinforced plastic solar vehicle are detailed. In particular, the protocols used for the design of the lamination sequence of the chassis, the leaf springs structural analysis, and the crash test numerical simulation of the vehicle, including the safety cage, are described. The complexity of the design methodology of fiber-reinforced composite structures is compensated by the possibility of tailoring their mechanical characteristics and optimizing the overall weight of the car.

Video Link

The video component of this article can be found at <https://www.jove.com/video/58525/>

Introduction

A solar car is a solar-powered vehicle used for land transport. The first solar car was presented in 1955: it was a tiny 15-inch model, made up of 12 selenium photovoltaic cells and a small electric motor¹. Since that successful demonstration, large efforts have been made worldwide to prove the feasibility of solar-sustainable mobility.

The design of a solar vehicle² is severely restricted by the amount of energy input into the car, which is quite limited in ordinary conditions. Some prototypes have been designed for public use, although no cars primarily powered by the sun are available commercially. As a matter of fact, solar cars seem far from a common use in everyday life given their current limits, especially in terms of cost, range, and functionality. At the same time, they are representing a valid test bench for the development of new methodologies, at the levels of both design and manufacturing, combining technology typically used in advanced industrial sectors, such as aerospace, alternative energy, and automotive. In addition, most solar cars have been built for the purpose of solar car races, blazoned events all around the world, whose participants are mainly universities and research centers that are boasting the research of optimal solutions for each technical problem. In particular, the organizers of the most important competitions (e.g., the World Solar Challenge) have been adopting a strategy of development of the race regulations that aim to bring these extreme vehicles as close as possible to the more traditional means of transport. Specifically, after many years in which the vehicles were single-seaters and designed to travel the route as quickly as possible, the emergent category of cruiser vehicles has been recently introduced and developed for the efficient transport of more passengers.

For these vehicles, the technical requirements have become even more stringent. In fact, not only do they have to guarantee the maximum energy efficiency, but they must also comply with more complex engineering conditions linked to different functionalities. For example, the possibility of transporting a greater number of occupants makes it more difficult to guarantee the conditions of safety and drivability. The endeavor is made more complicated due to the overall weight increase and the need to insert a much larger battery pack, while internal spaces must be reduced, making the positioning of the mechanics difficult.

A new design philosophy must be approached, including a different vision of material use and manufacturing. First, materials must be selected based on the highest strength-to-weight ratio and, as a direct consequence, carbon-reinforced fiber plastics represent an optimal solution. Furthermore, specific stratagems in the design must be implemented.

In the present article, the procedures employed to design some of the most important structural parts of the solar vehicle, such as its monocoque chassis, the suspension, and even a computational crash test are depicted. The final scope is to obtain rapidly a solar vehicle with the least possible weight, in a trade-off with aerodynamics and race rules.

Obviously, the search for the optimum material in terms of the ratio between resistance and weight is constrained by the technology employed, which is the autoclave molding of CFRP prepregs. The aim of the selected methods is the rapid determination of the optimal material choice in terms of ply typology within a finite range of possibilities and in terms of lay-up. In fact, designing with composite materials implies the simultaneous choice of the sections' geometrical properties, of the specific material, and of the suitable technology (that, in the case presented here, was determined *a priori*, as often happens).

Several renowned long-distance performance competitions for solar electric vehicles have been held worldwide in the last decades, involving top-rank universities and research centers, who are the main promoting agents for the development of such mobility technology. However, the competitiveness that runs in this research field in alliance with intellectual property boundaries is a seriously limiting factor for the diffusion of knowledge on the matter. For this reason, the literature review on solar car design accounts for few (and sometimes outdated) references, even when entire researches are based on this survey³, which is why the realization of works such as the present are encouraged.

Independently of which aspect of the vehicle's design is being improved, a common objective is always aimed at: the attainment of more energy efficiency. Productive changes in design are not always based on cutting-edge technologies, as they can be merely based on mechanics such as lowering the center of gravity of the vehicle to increase its stability (which is particularly important for competitions held in desert regions⁴ due to side wind gusts⁵) or reducing the weight of vehicle parts⁶-of which a 10% of overall weight reduction in electric vehicles can infer up to 13.7% in energy saving⁷. Thorough energy management strategies are also commonly used in race events to assure the best possible performance, where exciting maximum speeds of 130 km/h and single charges that last for over 800 km can be obtained in cruiser-class cars⁸.

The study of the vehicle's aerodynamics^{5,9,10} is important to assure little resistance from air and smoothness during driving, where the main aspects to be controlled are a reduction of the drag coefficient to allow the car to move while spending less energy, and the lift coefficient that must be kept negative to guarantee that the car is safely and stably attached to the ground, even at higher velocities.

Another important parameter to be designed is the suspension system, which is generally applied in regular vehicles with the sole purposes of providing comfort, stability, and safety, but in solar cars it must also be light. This important aspect has been explored since 1999¹¹ in studies involving fiberglass leaf springs and, more recently, with carbon fiber¹² which, when used to constitute wishbone links¹³, has proven to provide not only weight reduction but also an enhanced safety factor. Although double-wishbone suspensions are undoubtedly more often used in solar cars¹⁴, the current study considers a transversal leaf spring built with carbon fiber, for it is a simpler and lighter suspension system with reduced unsprung weight.

As for the manufacture of the chassis, the construction of a monocoque structure made of carbon fiber has proved to grant a significant performance advantage, being an indispensable design constraint for the most prominent existing^{4,8,15} solar car teams. The usage of carbon fiber is vital to the execution of the vehicle, allowing the teams to build vehicles where each one of the structural components (or different parts of the same structure, as in the chassis) has an optimal amount of fibers layered in calculated orientations. For that, in this work, the material properties have been assessed through standardized experimental tests, such as the three-point bending test and the interlaminar shear strength (ILSS) test.

To assure dimensional stability during the cure cycle, the construction is generally made with vacuum bagging and autoclave molding⁴ on carbon fiber molds which, in their turn, are laminated on precisely milled high-density foam or aluminum patterns. The majority of the parts is constituted by sandwich structures (*i.e.*, with fibers on the skin and extremely light-weight core materials that serve to attribute the bending resistance to the composite carrying an extremely low weight). In addition, carbon fiber is also advantageous for offering higher vibrational safety levels against resonance phenomena¹².

Aiming to certify the safety of the passengers in crash events, crash tests usually involve time-consuming and uneconomical, experimental, and destructive tests with sample vehicles. One recent trend that is gaining vast popularity is computer-simulated crash testing, where these simulations investigate the safety of the car occupants during different kinds of impacts (*e.g.*, full frontal, offset frontal, side impact, and roll over). Given the importance of performing a crash analysis on a road vehicle and the feasibility of doing so through numerical modelling, the present investigation aims at identifying the most critical areas of the solar vehicle, in terms of both maximum stress and deformation, in order to allow a hypothesis of improvement of the structure.

The numerical crash test on solar vehicles hereby carried out is unprecedented. Considering the lack of bibliography on research and the specific regulations for this innovative solar car approach, an adaptation that considers the impact of the vehicle on a rigid obstacle at its average speed was assumed. For that, the geometry modelling of the vehicle and the simulation (including mesh constitution and simulation set-up) have been conducted on different appropriate software. The usage of carbon fiber for the vehicle's structure is also justified by its crashworthiness behavior, which has already been shown to be higher than that of other materials, such as glass fiber composites, on crash tests of electric vehicles¹⁶.

Protocol

NOTE: The design process of a solar vehicle is a quite complex task, involving multidisciplinary aspects, so it is not possible to cover them all here. In order to guide the reader, the logical process in which the described protocols are embedded is shown in **Figure 1**.

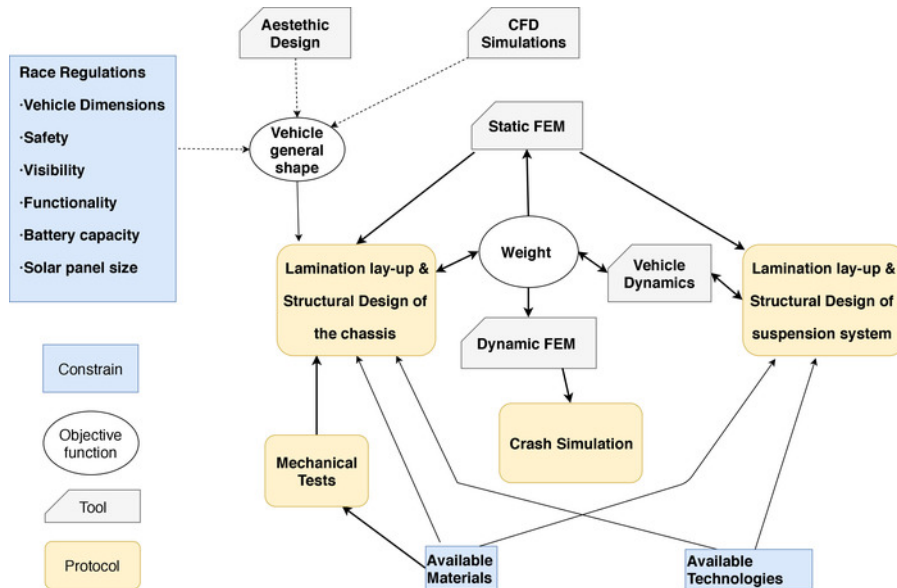


Figure 1: Design flow chart. The interactions between the different parts of the design process are depicted. [Please click here to view a larger version of this figure.](#)

1. Lay-up of the Main Chassis Design

1. Determine the load distribution in the worst-case scenario.
 1. Multiply the passengers' and battery pack mass distributions by the design's vertical acceleration to obtain the main design load.
 2. Consider the position of the seats and the different possible battery locations.
2. Calculate the reactions on the leaf spring joints. The vehicle is considered as a simply supported a-beam.
3. Determine the diagrams of the bending moment and shear.
4. Find the maximum allowable shear stress on the core material. Its value can be read in the core technical sheet or found by means of experiment on suitable specimens. In this case, the delamination stress of the core plies can be determined.
5. Calculate the sandwich core thickness based on the shear resistance^{17,18} (where w is the width over which the shear force T is applied and t_c is the core thickness).

$$\tau = \frac{T}{w \cdot t_c}$$

6. Find the tensile and compressive strength of the available CFRP plies. Their value can be found in the plies' technical sheets.
7. Determine experimentally the bending strength of the sandwich composites¹⁹.
8. Determine experimentally the ILSS for the possible combinations of materials^{20,21}.
9. Take into consideration the different sections of the vehicle, whose shape is designed in a trade-off between aerodynamic requirements and functional needs.
NOTE: There are three critical sections in the chassis—the one with the highest bending moment, and the two ends, where the area is dramatically reduced due to the presence of the wheel-suspension systems. Moreover, in these two reduced sections, the shear must be transferred from the leaf spring to the chassis.
10. Make an assumption about the lay-up in the three sections considered and in the different parts of the sections, taking into consideration that the technological minimum¹⁷ is at least 10% of the fibers in each direction (0° [*i.e.*, longitudinal], 90° [*i.e.*, transversal], and $\pm 45^\circ$ [*i.e.*, diagonal]), the most important load acting in the specific part of the section, that the number of plies is integer, and that the thickness must be kept to a minimum.
11. Calculate the maximum tensile and compressive stresses according to the sandwich theory^{17,18} and compare them to the allowable ones (where w is the width over which the moment M is applied and t_c and t_p are the thickness of the core and of the plies, respectively).

$$\sigma = \frac{M}{w \cdot t_c \cdot t_p}$$

1. Modify the lay-up, if necessary, and go back to step 1.9.
12. Make a finite element shell model in the software Abaqus and apply the impact-equivalent loads prescribed by the regulations²².
 1. Create the chassis in a CAD modeler.
 2. Import the chassis in the FEM software as a shell or solid part by clicking on **Import | Part**. If it is imported as a solid, use the **Geometry Edit** tool to transform it into a shell part.
 3. Define the properties of a single CFRP ply as **Elastic** material with type **Lamina** or **Engineering Constants**; select the elastic moduli and Poisson's ratios of the material. Notice that engineering constants parameters are needed if the out-of-plane behavior of the shell is analyzed. Choose **Hashin Damage Criterion** to implement a failure criterion for the composite ply²⁶.
 4. Create a **Composite Layups** section by defining the stacking sequence of the laminate. Assign each ply its orientation and thickness in tabular form.

NOTE: The post-curing thickness must be considered for the CFRP plies.

5. Assign the distribution of discrete elements of the part by **Mesh Seed**. Use the **Partition Face** tool and **Bias** seed to increase the number of elements at the critical locations. Choose the **Quad-dominated** element shape and the **Shell** element type. Click on **Reduced integration** if the hourglass effects in the model are negligible; otherwise, use nonreduced integration.
 6. Create an instance of the chassis in the **Assembly** module. This is the one to which the loads and boundary conditions will be applied.
 7. Define the analysis procedure in the **Step** module as **Static**. Choose the settings of the solver. Select **Nlgeom: On** to activate nonlinear membranial behavior.
 8. Apply loads that are equivalent to the ones prescribed by the regulations as **Body force** loads on the chassis. Apply **Concentrated forces** at the batteries' and occupants' positions to take into account their lumped weights.
 9. Apply the **BCs** on the instance. Consider the chassis as a supported body acted upon by the external loads, with **Pinned BC** at the constrains' locations.
 10. Define the outputs in the **Field Output Requests** module. Select **Domain: Composite layup** to extract the outputs at each ply's location in the laminate.
 11. Create a **Job** and run the analysis.
 12. Verify the compliance of the results with the regulations' requirements²². In case they are not fulfilled, go back to Steps 1.9 and 1.12.4 and modify the lamination sequence.
13. Produce a ply-book translating the section-by-section approach of the structural designer to a ply-by-ply approach needed by the manufacturer.
 1. Make special modifications in the sections where specific functional requirements lead to a reduction of the sandwich thickness.
 14. Manufacture the chassis in an autoclave.
 1. Produce high-density foam patterns by precision milling.
 2. Guarantee a smooth surface finish with fine-granulometry sandpaper.
 3. Apply layers of sealer and release agent on the foam to assure the detachability of the carbon fiber molds.
 4. Manufacture the molds by assembling pre-impregnated low-catalysis-temperature carbon fiber layers and sealing each part with vacuum bag compression for a further autoclave cure.
 5. Polish the surface of the produced molds and apply sealer and release agents.
 6. Laminate the chassis parts over the mold according to the ply-book and submit them to vacuum bag compression and an autoclave cure.

2. Leaf Spring Design

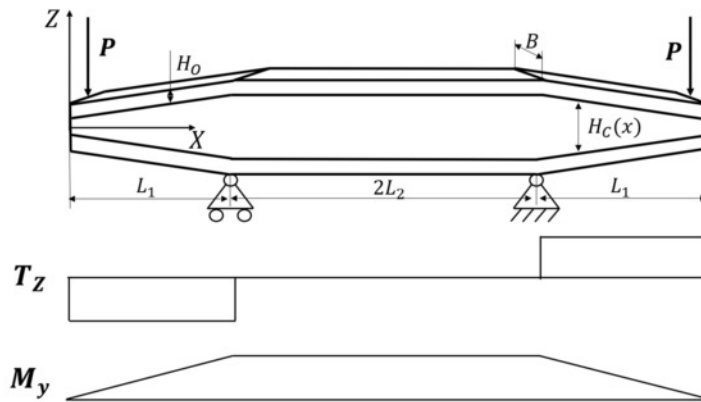


Figure 2: Loading diagrams of the leaf spring. This figure shows the determination of the shear and of the bending moment acting on the leaf spring. [Please click here to view a larger version of this figure.](#)

1. Determine the load distribution along the leaf spring (see the bending and shear diagram of **Figure 2**).
 1. Evaluate the maximum load applied at the wheels of the vehicle in the worst-case scenario (see Step 1.1).
 2. Calculate the reactions forces (maximum load P_{max}) on the leaf spring ends, considering the suspension arm leverages.
 3. Define the supporting and loading points of the leaf spring based on its anchorage points to the vehicle chassis and the suspension ones.
 4. Determine the diagrams of bending and shear, modeling the leaf spring as a four-point bending beam with an equal maximum load applied at the ends (worst-case scenario).

- Evaluate the maximum displacement δ_{max} of the leaf spring ends in accordance with suspension geometry and allowable space around the vehicle frame.
- Select the material with the higher specific strain energy-storing capability, γ .

$$\gamma = \frac{1}{2} \cdot \frac{\sigma_t^2}{\rho E}$$

Here, σ_t is the allowable stress, E is the elastic modulus, and ρ is the density.

- As bending is the dominant load of the leaf spring (the shear load is one or two orders of magnitude lower), keep the fatigue strength of the material as σ_t .
 - For composite orthotropic materials, consider the fatigue bending strength of the FRP along the principal direction (fiber direction) as σ_t .
- Conceptually design the leaf spring shape and lay-up, to maximize its specific energy storing capability.

NOTE: The leaf spring cross section should be modeled so that the maximum allowable stress state occurs along all the leaf spring.

- Focus only on the bending diagram of **Figure 2**. The shear load is one or two orders of magnitude lower. Based on that, divide the leaf spring in two types of sectors: between the two supports (L_2) and between the supports and the leaf spring ends (L_1).
- Along L_2 , keep the bending load constant and at its maximum; hence, also keep the cross-section constant.
- Along L_1 , increase the bending load linearly from the load application point to the support; hence, the cross-section height $H(x)$ should satisfy the following equation to keep the stress σ constant on the outer surface of the leaf spring, along all its length.

$$M(x) = Px = \sigma \frac{BH(x)^2}{6} \rightarrow h(x) \propto \sqrt{x}$$

Here, x is the distance from the point of application of the maximum load P and B is the cross-section width. The formula suggests that along the L_1 span, the leaf spring's cross-section height $H(x)$ should be tapered with a parabolic profile. However, for process practice reasons, approximate the leaf spring's height profile with a linear one.

NOTE: Keep B constant to avoid fiber interruption during the lamination process, which will reduce the strength of the composite laminas.

- Because bending is higher than the shear load, use a sandwich structure with a linearly tapered core of 0-90 fabric FRP to resist shear loads and confer torsional stiffness to the leaf spring and outer layers of unidirectional FRP oriented with the leaf spring's principal axis to contrast the bending load. The outer layers have a constant thickness to avoid geometrical discontinuities in the higher stressed zone.
- Obtain the tensile, compressive, flexural, and shear strength of the selected FRP materials. Their value can be found in the technical data sheets or by means of a test based on ASTM standards (preferred option).
 - Optimize the leaf spring geometrical dimensions by means of an analytical model.

NOTE: The objective function is to minimize the mass while complying to the imposed constraints; hence, sustain a maximum load P_{max} with a deflection equal to δ_{max} and keep the stresses lower than the material-allowable ones.

- Constrain the condition on the maximum deflection δ_{max} for a specified max load P_{max} .

$$\delta_{max} - \varepsilon \leq \delta(P_{max}) \leq \delta_{max} + \varepsilon$$

Here, ε is a small value inserted for convergence reasons. Conceptually, the leaf spring is a sandwich with a tapered core in the L_2 region. Calculate the deflection δ at the loading P , by means of Castigliano's method.

$$\begin{aligned} \delta &= \frac{\partial U}{\partial P} = \frac{\partial}{\partial P} \left(\int_0^{L_1} \frac{M^2(x)}{2D_1(x)} dx + \int_{L_1}^{L_1+L_2} \frac{M^2(L_1)}{2D_2} dx \right) \\ &= \frac{\partial}{\partial P} \left(\int_0^{L_1} \frac{(Px)^2}{2D_1(x)} dx + \int_{L_1}^{L_1+L_2} \frac{(PL_1)^2}{2D_2} dx \right) \\ &= \frac{\partial}{\partial P} \left[\frac{P^2}{2} \left(\int_0^{L_1} \frac{x^2}{D_1(x)} dx + \int_{L_1}^{L_1+L_2} \frac{L_1^2}{D_2} dx \right) \right] \end{aligned}$$

Here, $D_1(x)$ and D_2 are the flexural stiffness of the leaf spring along L_1 and L_2 , respectively.

$$D_1(x) = \frac{B}{12} (H_C(x)^3 (E_C - E_O) + (H_C(x) + 2H_O)^3 E_O) \text{ and } D_2 = D_1(L_1)$$

Here, E_C and E_O are the elastic modulus of the core and the outer layers, respectively, H_O is the outer layer thickness, and $H_C(x)$ is the core thickness.

$$H_C(x) = H_{Cmin} + \frac{H_{Cmax} - H_{Cmin}}{L_1} x \text{ for: } 0 < x < L_1$$

$$H_C(x) = H_{Cmax} \text{ for: } L_1 < x < L_2$$

- Constrain the condition on the maximum bending stress: $\sigma_f < \sigma_{11}$ (maximum UD fatigue bending stress). Evaluate σ_f by means of the Euler-Bernoulli theory.

$$\sigma_f = \frac{P_{max} L_1}{D_1(L_1)} \left(\frac{H_C(L_1)}{2} + H_O \right) E_O$$

3. Constrain the condition on the maximum core and outer layer shear stresses: $\tau_{core} < \tau_{13core}$ (maximum core fatigue shear stress) $\tau_{out} < \tau_{13out}$ (maximum core fatigue shear stress). Evaluate τ_{core} and τ_{out} by means of the Euler-Bernoulli theory²⁴.

$$\tau_{core} = \frac{P_{max}}{2 D_1(0)} \left(E_C \frac{H_C(0)^2}{4} + E_O H_O (H_O + H_C(0)) \right)$$

$$\tau_{out} = \frac{P_{max} E_O}{2 D_1(0)} \left(\frac{H_C(0)}{2} + H_O \right)^2$$

4. Use the leaf spring mass as objective function to minimize.

$$Mass = \left(\int_0^{L_1} H_C(x) \rho_C + 2H_O \rho_O dx + \int_{L_1}^{L_1+L_2} H_C(L_1) \rho_C + 2H_O \rho_O dx \right) 2B$$

NOTE: The geometrical parameters which can be varied are: H_C , H_O , and B . If allowed by the design of the anchorage points to the frame, L_1 and L_2 can also be considered as variables, if the following constrain is respected: $L_1 + L_2 = const$.

5. Solve the problem iteratively or by means of optimization algorithms, which can be found integrated in several numerical computing software programs.
7. Perform an FE simulation of the optimized leaf spring in **Ansys Composite Pre/Post (ACP)**. The goal is to evaluate the stress concentration and the out-of-plane loads.
 1. Draw, as a surface, the CAD geometry of only one quarter of the leaf spring, with the surface divided in correspondence with the support point and lay-up variations.
 2. Create a new simulation project in the **ANSYS Workbench**. Select **ACP (Pre)** (in the **Toolbox** menu) by dragging it into the workspace.
 3. Define material properties by clicking on **Engineering Data**. Select **Engineering data sources** and import from the **Composite materials** folder carbon UD and woven prepreps default material properties, by double-clicking on them. Update the material constants in the three principal directions with the ones available on the material data sheet or obtained from experimental results.
 4. Import the geometry while keeping the link with the CAD by right-clicking on **Geometry** and then on **Import geometry**. Import it in the native CAD format.
 5. Double-click on **Model**. Assign an arbitrary surface thickness. Define the different layup zones by using the **Named Selection** function (right-click on **Model** and then on **Insert**). Generate the default mesh by right-clicking on **Mesh** and then on **Generate mesh**.
 6. In **Workbench**, open **ACP-Pre** by double-clicking on **Setup**.
 7. Define the plies' properties in the **Material Data** menu folder. Select **Create Fabric** by right-clicking on **Fabrics**; then, define the **Material** and assign the prepreg **Thickness**. Select **Create Sub laminates** by right-clicking on **Sub Laminates** and define the sub-laminate stacking sequence.
 8. Define the element local coordinates system in the **Rosettes** menu folder according to the principal direction of the lamination process (principal leaf spring axis).
 9. Orient the local coordinates of the FEM elements in the **Oriented Selection Set** menu folder by defining for each **Element sets** (previously defined in Step 2.7.5) an arbitrary origin **Point** and the **Rosettes** set in Step 2.7.8.
 10. Define the layup based on the results obtained in the optimization process of Step 2.7. Right-click on **Modeling Groups** and select **Create Ply**. Define the **Oriented Selection Set**, the **Ply material**, and the **Number of Layers**. Repeat it for each repeating group of plies.

NOTE: Follow the same stacking order of the lamination process.
 11. In **Workbench**, drag **Static structural** analysis (in the **Toolbox** menu) onto the workspace. Then, drag **ACP (Pre)\Setup** on **Static structural\Model** and select **Transfer solid Composite Data**. Double-click on **Static Structural\Setup**.
 12. Apply the symmetry and constrain boundary condition. Right-click on **Static Structural** and select **Insert\Displacement**. Select the **Edge** or the **Surface** of the **Geometry** and set the displacement to 0 for the appropriate **Component** direction.
 13. Apply the **Force** following the same procedure of Step 2.7.12.
 14. Solve the FEM model as linear elastic by clicking on **Solve**.
 15. Evaluate the maximum displacement (δ_{max}) of the leaf spring by right-clicking on **Solution** and selecting **Insert\Deformation \Directional**. If it is low, come back to Step 2.7.10 and increase the number of the outer UD plies; if it is higher, reduce it.
 16. In **Workbench**, drag **ACP (Post)** (in **Toolbox**) on the **ACP (Pre)\Mode**. Then, drag **Static\Structural** solution on **ACP (Post)\Results**. Double-click on **ACP (Post)\Results**.
 17. Right-click on the **Definition** menu folder and select as failure criteria **Hashin 3D**.
 18. Right-click on the **Solutions** menu folder and select **Create Failure** Select **Hashin** and check **Show on Solids**.
 19. Check if the failure criteria are always below one. If they are not, go back to Step 2.7.7 and increase the number of plies in the zone identified as critical, orienting them as necessary.
 20. Write the ply book.
8. Test a scaled model of the designed leaf spring.
 1. Design, by means of the analytical model of Step 2.7, a 1/5- to 1/10-scaled leaf spring, tuning the outer layers and core thickness to have the same ratio between bending and shear stress of the real component and a similar curvature for the maximum load.
 2. Laminate the scaled leaf spring.

3. Test it with an ordinary four-point bending test fixture.
 4. Analyze the maximum load and displacement and the failure mode.
 5. Optimize the design of the leaf spring based on the conclusions of the experimental test.
9. Manufacture the optimized leaf spring.

3. Full-Frontal Crash Test Simulation

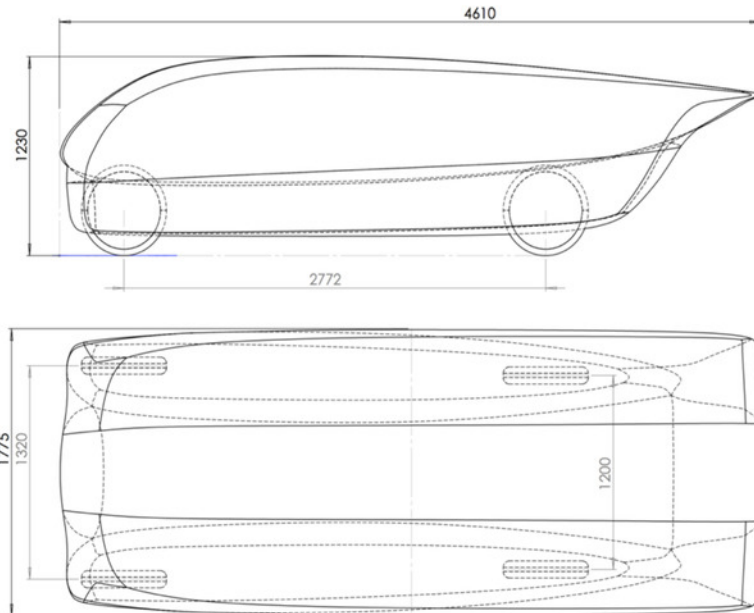


Figure 3: Cruiser geometry. This figure shows the general shape and dimensions of the vehicle. [Please click here to view a larger version of this figure.](#)

1. Draw the geometry of the vehicle (**Figure 3**).
 1. Create and name a new **Part** project in the CAD modeling software.
 2. Model solid parts using the resources **Extrude**, **Revolve**, **Swept**, and **Loft** to ensure full contact between different vehicle parts (such as chassis, seats, and roll cage). When necessary, click on the tab **Surface**, **Reference Geometry**, and **Plane** to draw a reference plane.
 3. Repeat Step 3.1.2 until the geometry is complete with monocoque, doors, roll cage, seats, battery, wheels, tires, wheel hubs, suspension arms, leaf spring, steering system, and rigid solid barrier (2 x 2 m).
 4. Exploit the bilateral symmetry to optimize calculations and use a half-car model. Under the **Utilities** tab, click on **Symmetry Check** and select the **Automatic Symmetry Split** command. Then, click on the part of the body that will be kept and confirm by clicking on **Split Part**.
 5. Convert the solid bodies into surfaces: select the faces related to the thickness of the bodies and click on the **Surfaces** tab and, then, on **Delete Face**.
 6. Click on **Save as** and select the **STP** format.
2. Set up and perform the simulation.
 1. Create and name a **New Project** in the ANSYS Workbench Finite Element simulation software.
 2. Drag from the **Toolbox - Analysis Systems** to the Project Schematic an **Explicit Dynamic** window. Double-click in **Engineering Data** and add new materials, dragging their necessary properties from the **Toolbox** tree and inserting the values obtained in Section 1 of this protocol, naming each material accordingly.
 3. Right-click on **Geometry** to **Import Geometry**. Click on **Browse** and select the STP file generated in Step 3.1.6.
 4. Double-click on **Model** under **Explicit Dynamic** to open the **Model** environment.
 5. Once inside the **Model** environment, right-click on **Geometry** to insert **Point Mass** for 3-D elements or in **Layer Section** for 2-D elements, to define concentrated masses or the composite layup, respectively. For each component under **Geometry**, the proper material and thickness of the surfaces should be assigned under **Detail-Materials**.
 6. Right-click on **Model** to insert **Symmetry - Symmetry Region**. The YZ symmetry plane defines correct geometrical symmetry in terms of the future results giving proper boundary conditions.
 7. To correctly set up **Connections**, delete all automatic connections and leave only **Body Interactions**, defined as frictionless.
 8. Under the details of the **Mesh Explicit Method (Figure 4)**, drop the **Elements midside nodes** and set up the **Sizing function** on **Curvature** with **Medium Relevant Center**. Set up the Maximum Element Size to 30 mm with a minimum of 6 mm.
 9. Set the **Number of CPUs** for parallel processing under the **Advanced** tab of the **Mesh** section.
 10. Set the **Velocity** as an initial condition under the **Initial Conditions** tree of the **Explicit Dynamics** tab.
 11. Set the constraint boundary conditions by right-clicking on the **Explicit Dynamics** tab, selecting **Insert**, and picking **Fixed Support** to define the rigid barrier and **Fixed Displacement** to prevent that the wheel moves on the Z-axis.

12. Under **Analysis Settings**, set up controls in terms of **End Time** (to 0.3 s) and **Maximum Number of Cycles** (to 2.5×10^5), the necessary inputs to obtain velocity, and the Kinetic Energy (equal to zero).
13. Under **Solution**, right-click on **Solution Information** to insert **Kinetic – Total - Internal Energy** to track these results. On the other side, under **Solution Information**, **Solution Output** can be tracked in terms of **Energy Summary**, **Time Increment**, and **Energy Conservation**.
14. Click on **Solve** and analyze the outcome results in terms of Total Deformation, Stress, Strain, Total, Internal and Kinetic Energy, and Acceleration.

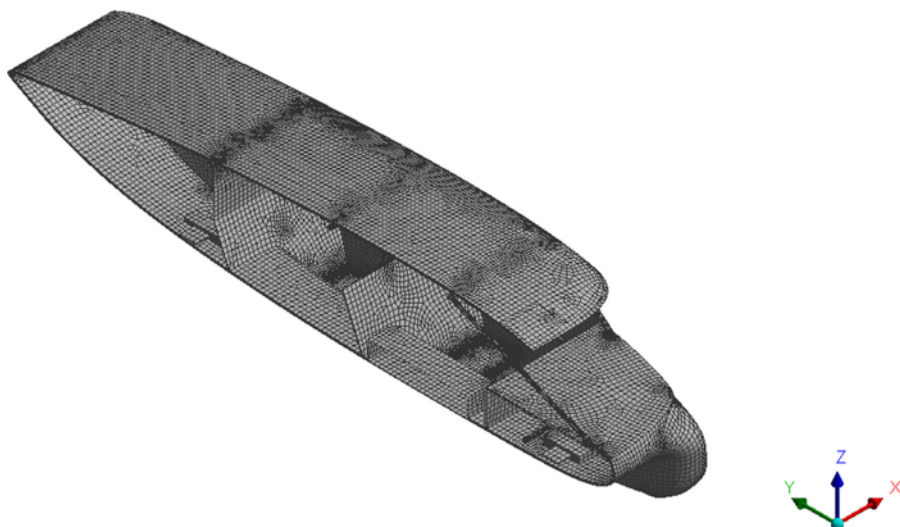


Figure 4: Mesh of the finite elements applied to the half-vehicle model. This figure shows the discretization of the model, done of on half of the vehicle due to symmetry. [Please click here to view a larger version of this figure.](#)

Representative Results

Lay-up of the Main Chassis: The final outcome of the protocol is the lamination sequence, also called the ply book. However, while the load distributions and the diagrams of the bending moment and shear force may be determined by simple solid mechanics considerations, a key point of the protocol is the evaluation of the actual material properties. In fact, even if many of the quantities needed by the structural designer can be found in the material data sheet, the manufacturing phase and the interaction with other materials can change the mechanical response of the raw materials. In this section, the experimental set-up for the three-point bending and the ILSS tests are shown (see **Figure 5**). From these tests, it is possible to evaluate the bending strength of the sandwich laminas and to find a lower limit for the shear strength of the Nomex core; representative stress-displacement curves are shown in **Figure 6** for two different orientations of a woven laminate. Moreover, the ILSS is critical to determine the resistance to delamination in the chassis edges, where the sandwich becomes a laminate.

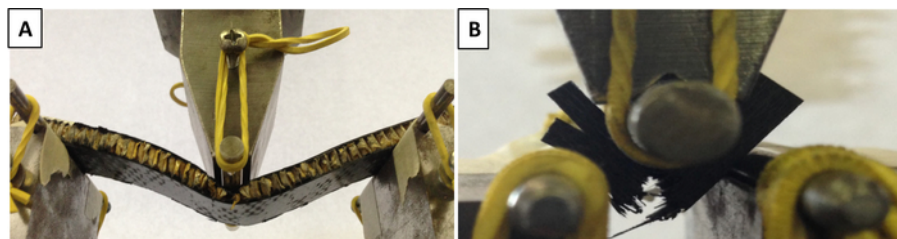


Figure 5: Mechanical tests. These panels show mechanical tests of (A) the three-point bending and (B) the ILSS. The specimen's shape and the loading conditions are shown. [Please click here to view a larger version of this figure.](#)

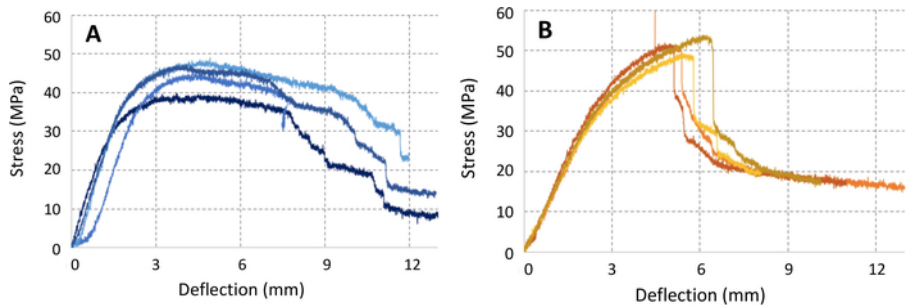


Figure 6: Typical result of three-point bending tests. These panels show typical results of a three-point bending test for (A) $[0/90]_n$ plies and (B) $[\pm 45]_n$ plies. Stresses calculated from the load are measured by the load cell and the displacement is measured by the transducer embedded in the testing machine. [Please click here to view a larger version of this figure.](#)

In **Figure 7**, the lamination sequences, defined sector by sector over the chassis mold, are shown. The detailed specification of the lamination sequences is listed in **Table 1**. The table is divided into the three phases of the autoclave curing process that are done in sequence, starting from the outermost lamina, then the Nomex core and the adhesives, and finally the inner lamina.

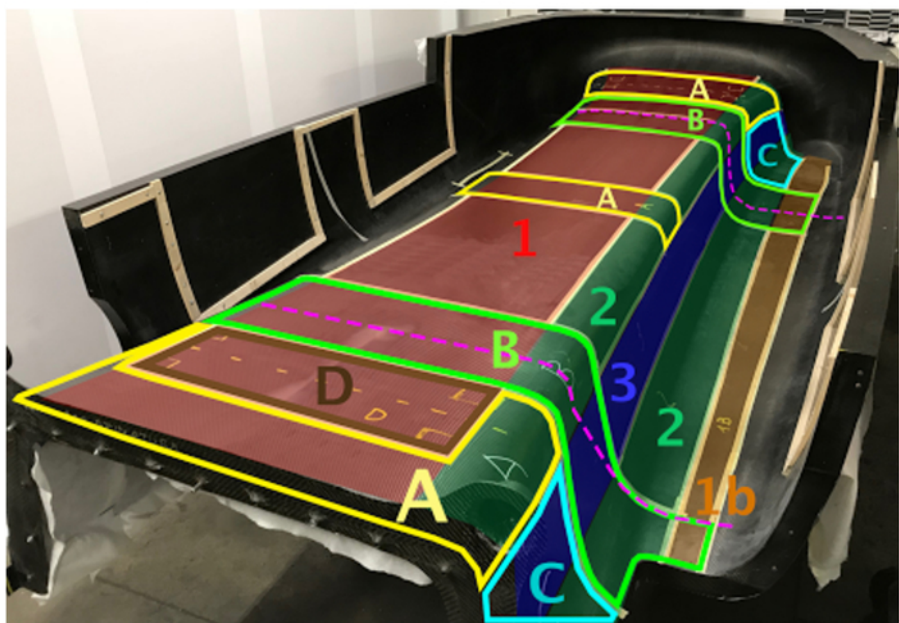


Figure 7: Result of the design process. Every area is characterized by a different lay-up. The numbers and the colors define the different regions in which the chassis structure is divided, see **Table 1**. [Please click here to view a larger version of this figure.](#)

Phase 1				
<i>p = 6 bar; t = 2 h; T = 135 °C</i>				
Seq.	Sector	Angle	n°	Material
P 1.1	Global	+45°	1	satın T800
P 1.2 (reinf)	1	0°	1	UNI M46J
	2	90°	1	UNI M46J
	3	+45°	1	UNI M46J
	1b	0°	1	UNI M46J
P 1.3 (reinf)	D	0°	2	UNI M46J
	C	-45°	1	UNI M46J
	C	+45°	1	UNI M46J
	A, B, C, D	-45°	1	UNI M46J
	A, B, C, D	+45°	1	UNI M46J
P 1.4 (reinf)	B	0°	2	UNI M46J
	A, D, C	90°	1	UNI M46J
	A, D	90°	2	UNI M46J
P 1.5 (reinf)	D	0°	1	satın T800
	D	90°	3	UNI M46J
	D	0°	1	satın T800
	D	0°	3	UNI M46J
P 1.6	Global	0°	1	satın T800
Phase 2				
<i>p = 1,5 bar; t = 2 h; T = 1110 °C</i>				
P 2.1	Global	/	1	Adhesive film
P 2.2	1, 2, 3	/	1	nomex 14 mm. 32Kg/m ²
P 2.3	1b, D, 0	/	1	nomex 9 mm. 32Kg/m ²
P 2.4	Global	/	1	Adhesive film
Phase 3				
<i>p = 6 bar; t = 2 h; T = 135 °C</i>				
P 3.1	Global	0°	1	satın T800
P 3.2 (reinf)	D	0°	3	UNI M46J
	D	0°	1	satın T800
	D	90°	3	UNI M46J
	D	0°	1	satın T800
P 3.3 (reinf)	A, D	90°	2	UNI M46J
	A, D, C	90°	1	UNI M46J
	B	0°	2	UNI M46J
P 3.4 (reinf)	A, B, C, D	+45°	1	UNI M46J
	A, B, C, D	-45°	1	UNI M46J
	C	+45°	1	UNI M46J
	C	-45°	1	UNI M46J
	D	0°	2	UNI M46J
P 3.5	1b	0°		UNI M46J
	3	-45°	1	UNI M46J
	2	90°	1	UNI M46J

	1	0°	1	UNI M46J
P 3.6	Global	+45°	1	satin T800

Table 1: Lamination sequence of the chassis. This table shows the specification of the lay-up for the different areas of the chassis, defined in **Figure 7**. It is divided into three different lamination phases that are done in sequence.

Once the structure of the chassis is determined, a titanium roll cage is added according to the race's rules²⁰, and specific numerical tests are run to verify the resistance of the vehicle as a whole and, mostly, the absence of intrusion of nonstructural parts towards the occupants. In **Figure 8**, the directions of the impact-equivalent static loads are shown, and in **Figure 9** the corresponding displacement maps can be evaluated. In this phase, only a schematic geometry is used for calculation, while the complete geometry is used for the final verification of the crash test.

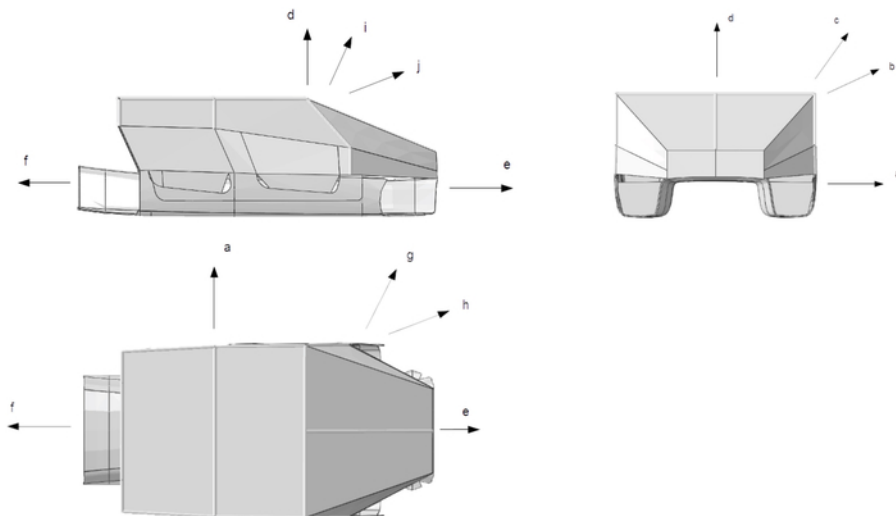


Figure 8: Crash-equivalent static load directions. According to the regulations, the vehicle structure is loaded by a static force equal to 6 times the total mass in the directions shown in the picture. [Please click here to view a larger version of this figure.](#)

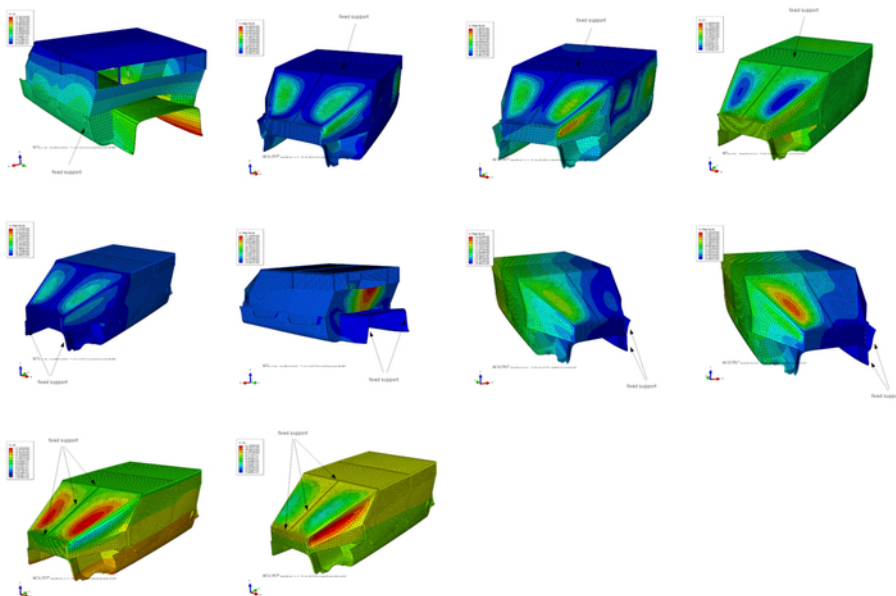


Figure 9: Map of the computed displacements. This figure shows an example of the displacements computed in the cases defined in **Figure 8**. The displacement must be lower than 25 mm in any region in the proximity of the occupants. [Please click here to view a larger version of this figure.](#)

Leaf Spring: The outcome of the protocol is the optimization of a composite transverse leaf spring with anti-roll capability. Its design has to meet different specific requirements: a stress below the material-allowable one for maximum load, a specific stiffness, and a minimum weight. In order to meet all of these requirements, an optimization analytical model is presented. Thanks to the model, it is possible to rapidly obtain the optimum geometry and conceptual lay-up. The accuracy of the model has been verified by the finite element method and an experimental test on a 1/5-scaled leaf spring. The scaled leaf spring is double-supported at the center (which spans 100 mm) and loaded at the ends corresponding to the holes (which span 190 mm) with 1,000 N for each side. The optimized geometry and ply-book of the leaf spring are reported in **Figure 10** and **Table 2**, respectively.

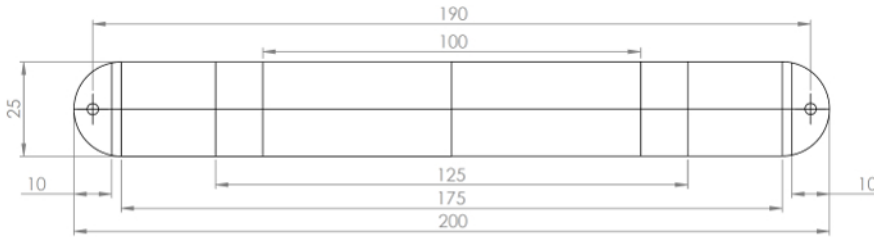


Figure 10: Optimized sample of the leaf spring geometry. This figure shows the geometry of the scaled leaf spring that is tested to fracture to validate the numerical model. [Please click here to view a larger version of this figure.](#)

Autoclave Curing					
$p = 6 \text{ bar}; t = 2 \text{ h}; T = 135 \text{ }^\circ\text{C}$					
Seq.	Sector	Angle	n°	Thickness	Material
				mm	
Ends 10	Ends 10	0°	1	0.23	TW T300 200g/m ²
All 200	All 200	0°	#	1	UD T1000 100gm/m ²
Central 125	Central 125	0°	1	0.23	TW T300 200g/m ²
Central 175	Central 175	0°	1	0.23	TW T300 200g/m ²
All 200	All 200	0°	1	0.23	TW T300 200g/m ²
Central 175	Central 175	0°	1	0.23	TW T300 200g/m ²
Central 125	Central 125	0°	1	0.23	TW T300 200g/m ²
All 200	All 200	0°	#	1	UD T1000 100gm/m ²
Ends 10	Ends 10	0°	1	0.23	TW T300 200g/m ²

Table 2: Lamination sequence of the leaf spring. This table shows the specification of the lay-up for the different areas of the leaf spring.

According to the analytical model, the leaf spring should have a maximum displacement of 12.2 mm and develop a maximum bending stress of 970 MPa, constant between the two central supports.

Finite element analysis as described in Step 2.7 of the protocol was performed and the results are reported in **Figure 11**. The stress in the principal direction σ_{11} on the outer surface of the leaf spring along its principal axis is plotted in the graph. It is almost constant between the span and equal to 922 MPa and, then, decreases linearly towards the load application point. Despite σ_{11} being far below the maximum compression tension of the material (1,450 MPa), the 3-D Hashin failure criterion plotted in **Figure 10** shows a zone with a failure index exceeding 1, which is caused by fiber failure (highlighted in red) and is associated to an abrupt change of geometry for the external UD plies, caused by ply interruption of the core. All the while, the displacement calculated by FEM at the load application point is 12.8 mm.

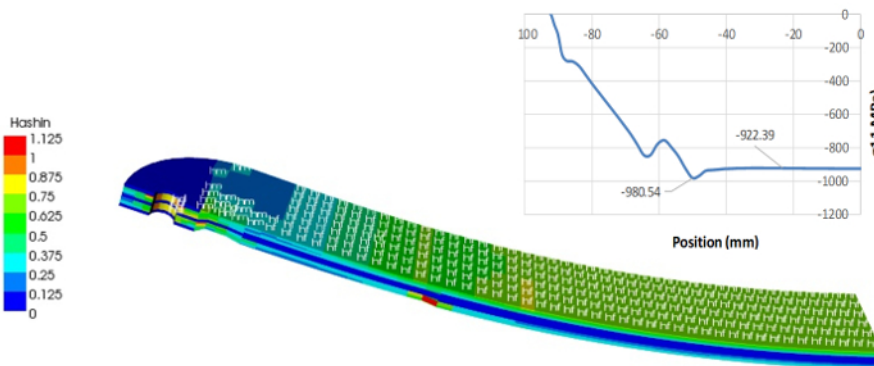


Figure 11: Bending numerical simulation on the leaf spring finite element model. This figure shows the results of the FEM simulation on the scaled leaf spring in terms of the Hashin failure index and maximum principal stress. [Please click here to view a larger version of this figure.](#)

In order to verify the reliability of the analytical and numerical models, as suggested by the procedure, the scaled leaf spring has to be experimentally tested. The results, reported in the graph of **Figure 12**, shows a maximum load before breakage of 1,980 N (990 N for each side), with a maximum displacement of 15.1 mm. Therefore, in terms of maximum displacement, the analytical and numerical model underestimate it by -19% and -15%, respectively. Interestingly, the failure mode and damage location observed on the tested specimen (**Figure 11**) agree with the numerical model results.

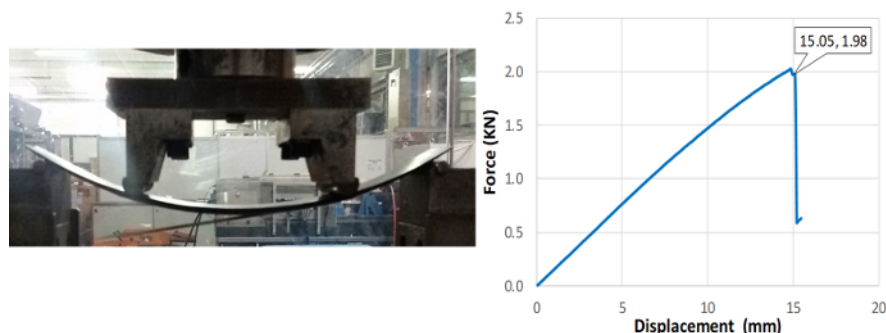


Figure 12: Four-point bending experimental test on a scaled model of the leaf spring. This figure shows the test set-up and load-displacement curve for the scaled leaf spring. [Please click here to view a larger version of this figure.](#)

Crash Test: Finite element analysis can produce realistic results to support engineers in understanding vehicle behavior under different crash scenarios. Instead of running real-life conditions, it is more time-efficient and cost-effective to simulate car crashes using commercial software such as ANSYS. The present results are an example of how these simulations can contribute to the automotive engineering community.

The discretized finite element model of the car presented a number of elements and nodes of 79950 and 79822, respectively. As an initial condition, it adopted a 60 km/h impact speed, where the kinetic energy of the vehicle decreased in approximately 0.3 s (**Figure 13**), being converted into contact and internal energy within the car structure.

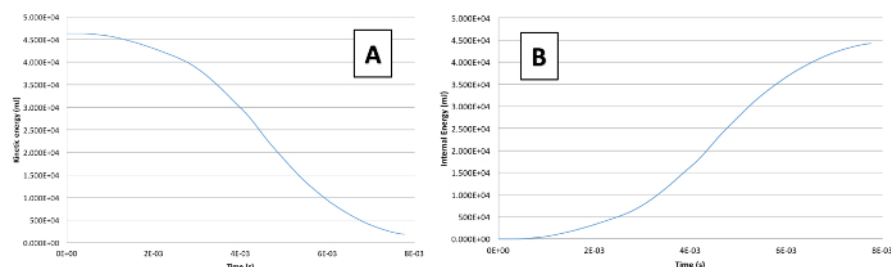


Figure 13: Crash test energy charts. These panels show the crash test energy charts of (A) kinetic energy and (B) internal energy. The charts portray typical energy fluxes during a crash event. [Please click here to view a larger version of this figure.](#)

From the sample stress map in **Figure 14A**, the status of the vehicle integrity can be assessed. This is of paramount importance to determine possible harm to the safety of the passengers, as it would be in the case of a potentially loosened roll cage bar, detachment of seats, or even a displacement of the steering bar towards the driver. The most prominent displacements in the case shown in **Figure 14B** are comprised within the 95 mm range, and occur both in the front of the car, due to the shock, and in the roll cage bars that are attached to the seats.

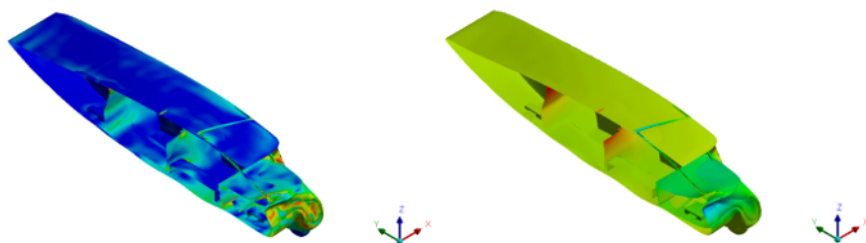


Figure 14: Typical contours of maximum equivalent stress and maximum displacement during a frontal crash test. These panels show (A) the equivalent stress and (B) the displacement. [Please click here to view a larger version of this figure.](#)

Discussion

From **Table 1**, it is possible to notice that the single laminas are not symmetrical, while the whole sandwich is. This is due to the necessity of having both the least number of plies, the technological minimum, and the desired mechanical properties.

On one side, the section marked as 1/1b, 2, 3 in **Figure 7** is responsible for the overall mechanical properties, being the orientation of the high-strength reinforcement unidirectional ply the main difference between them. On the other side, the sections marked as A, B, C, and D are

modified to take into account the concentrated loads of the suspension systems and of the passengers' seats, due to the presence of the leaf springs.

The finite element model used for the analysis of the composite chassis is based on a shell topology. Shell elements are a suitable option for reproducing composite structures, as they tend to capture the bending stiffness of thin-walled bodies with substantially simpler meshes than solid elements. On the other hand, resorting to continuum shell or solid elements should be considered when modelling thick sandwich structures or regions with steep stress gradients; a comparative discussion on shell and continuum shell elements is provided^{24,25}.

The main objective of the static analysis is verifying that the stiffness and strength of the structure meet the requirements. Stiffness requirements are enforced directly by ensuring that the deformation of the vehicle under each load case is within the limits of the regulations (*i.e.*, no part of the vehicle penetrates the occupants' room). Assessment of the structure's strength is based on evaluating Hashin's damage²⁶ of the composite plies; namely, Hashin's parameters must be strictly less than 1. As different damaging modes contribute to global failure of the composite laminate, the use of cumulative damage criteria (*e.g.*, Hashin's) is recommended; maximum stress criteria could be suitable for metallic components.

The literature has proposed various solutions for the design optimization of lightweight composite leaf springs, but most of them connect only a single wheel^{27,28} (no antiroll capability) or are only suitable for infusion mold technology (double-tapered)²⁹. The design of the leaf spring here presented is constrained *a priori* by the prepreg laminating process, which does not allow a double-tapered design solution but guarantees high material strength and reliability.

The innovative aspect of the leaf spring is the functional integration of two components in one (the spring and the antiroll bar) and the main advantage is the mass reduction. Moreover, thanks to the proposed analytical model, it is possible to further reduce the mass and get the optimal geometry fast for the set maximum load and displacement.

The local stresses and out-of-plane ones, which cannot be appreciated by the analytical model, are evaluated by the finite element method, and the leaf spring composite single layers are modeled with brick elements. This solution is computationally heavier than using shells but allows, in combination with Hashin, 3-D failure criteria to predict delamination caused by out-of-plane loads, which is a critical aspect of the leaf spring design. Finally, the analytical and numerical models for the design of the leaf spring have been validated by an experimental test on a scaled leaf spring.

Regarding the crash test, the relatively elevated displacement of the roll cage, although it does not represent a matter of concern, is mainly attributed to the layout of its front bar. Its noncurved shape and the acute way in which it is placed, with no curves and on a sharp angle with the impact direction, is responsible for transferring most of the energy that should be absorbed by the chassis to the roll cage, which has a distinct structural objective. For this reason, the roll cage is pushed to the rear of the vehicle, causing an elevated stress on its attachment regions to the seats. It is important to notice that, despite of any safety features that could be potentially improved upon, the minimal deformation of the monocoque and the fact that no components penetrated/perforated others make it clear that the design of the vehicle is considered safe regarding its crashworthiness.

Therefore, the structural design of the vehicle as a whole is considered to have been optimized in terms of material usage, where the extensive calculation showed in the protocol is essential for the design of a monocoque and for the leaf springs that were tailored to be light and to present an enhanced mechanical performance. Furthermore, through a numerical crash test simulation, the vehicle structure demonstrated that it is able to successfully withstand the momentum inferred by a full-frontal impact considering the average velocity of the car on its optimal energetic efficiency.

Disclosures

The authors have nothing to disclose.

Acknowledgments

The authors want to thank all members of the Onda Solare Sport Association (www.ondasolare.com) for their essential support and Marko Lukovic who was the aesthetic designer of the cruiser. This research activity was realized with the financial support of the European Union and of the Emilia-Romagna Region inside the POR-FESR 2014-2020, Axis 1, Research and innovation.

References

1. *Popular Mechanics Magazine*. **104** (3). Hearst Magazines (1955).
2. Thacher, E.F. *A Solar Car Primer, A Guide to the Design and Construction of Solar-Powered Racing Vehicles*. Springer (2015).
3. Minak, G., Fragassa, C., de Camargo, F.V. A brief review on determinant aspects in energy efficient solar car design and manufacturing. *Smart Innovation, Systems and Technologies*. **68**, 847-856 (2017).
4. Tamura, S. Teijin advanced carbon fiber technology used to build solar car for world solar challenge. *Reinforced Plastics*. **60**, 160-163 (2016).
5. Kin, W.D., Kruger, S., van Rensburg, N.J., Pretorius, L. Numerical assessment of aerodynamic properties of a solar vehicle. *ASME 2013 International Mechanical Engineering Congress and Exposition*. San Diego (2013).
6. Betancur, E., Mejía-Gutiérrez, R., Osorio-Gómez, G., Arbelaez, A. Design of structural parts for a racing solar car. In *Advances on Mechanics, Design Engineering and Manufacturing. Proceedings of the International Joint Conference on Mechanics, Design Engineering & Advanced Manufacturing (JCM 2016, 14-16 September, 2016, Catania, Italy)*. Edited by Eynard, B., Nigrelli, V., Oliveri, S.M., Peris-Fajarnes, G., Rizzuti, S., 25-32, Springer (2017).

7. Joost, W. Reducing vehicle weight and improving U.S. energy efficiency using integrated computational materials engineering. *Journal of the Minerals, metals, and Materials Society*. **64**, 1032-1038 (2012).
8. Paterson, G., Vijayarathnam, P., Perera, C., Doig, G. Design and development of the Sunswift eVe solar vehicle: a record-breaking electric car. *Journal of Automobile Engineering*. **230**, 1972-1986 (2016).
9. Betancur, E., Fragassa, C., Coy, J., Hincapie, S., Osorio-Gómez, G. Aerodynamic effects of manufacturing tolerances on a solar car. *Smart Innovation, Systems and Technologies*. **68**, 868-876, (2017).
10. de Kock, J.P., van Rensburg, N.J., Kruger, S., Laubscher, R.F. Aerodynamic optimization in a lightweight solar vehicle design. *ASME 2014 International Mechanical Engineering Congress and Exposition*. 1-8. Montreal (2014).
11. Sancrakter, E., Gratton, M. Design, analysis, and optimization of composite leaf springs for light vehicle applications. *Composite Structure*. **44**, 195-204 (1999).
12. de Camargo, F.V., Fragassa, C., Pavlovic, A., Martignani, M. Analysis of the suspension design evolution in solar cars. *FME Transactions*. **45** (3), 394-404, (2017).
13. Hurter, W.S., van Rensburg, N.J., Madyira, D.M., Oosthuizen, G.A. Static analysis of advanced composites for the optimal design of an experimental lightweight solar vehicle suspension system. *ASME 2014 International Mechanical Engineering Congress and Exposition*. Montreal (2014).
14. de Camargo, F.V., Giacometti, M., Pavlovic, A. Increasing the energy efficiency in solar vehicles by using composite materials in the front suspension. *Smart Innovation, Systems and Technologies*. **68**, 801-811, (2017).
15. Mathijssen, D. Redefining the motor car. *Reinforced Plastics*. **60**, 154-159, (2016).
16. Liu, Q., Lin, Y., Zong, Z., Sun, G., Li, Q. Lightweight design of carbon twill weave fabric composite body structure for electric vehicle. *Composite Structures*. **97**, 231-238 (2013).
17. Gay, D. *Composite Materials: Design and Applications*. CRC Press. Boca Raton, FL (2014).
18. Poodts, E., Panciroli, R., Minak, G. Design rules for composite sandwich wakeboards. *Composites Part B: Engineering*. **44** (1), 628-638 (2013).
19. ASTM D7264. Standard Test Method for Flexural Properties of Polymer Matrix Composite Materials. *ASTM International*. West Conshohocken, PA (2015).
20. ASTM D2344. Standard Test Method for Short-Beam Strength of Polymer Matrix Composite Materials and Their Laminates. *ASTM International*. West Conshohocken, PA (2015).
21. Rondina, F. *et al.* Development of full carbon wheels for sport cars with high-volume technology. *Composite Structures*. **192**, 368-378 (2018).
22. *American Solar Challenge 2018 Regulations. Revision B, September 4, 2017*. <http://americansolarchallenge.org/ASC/wp-content/uploads/2017/09/ASC2018-Regs-External-Revision-B.pdf> (2017).
23. Sodena, P.D., Kaddourb, A.S., Hinton, M.J. Recommendations for designers and researchers resulting from the world-wide failure exercise. *Composites Science and Technology*. **64**, 589-604 (2004).
24. Zenkert, D. *An Introduction to Sandwich Construction*. Engineering Materials Advisory Services Ltd (1995).
25. Barbero, E.J. *Finite Element Analysis of Composite Materials Using Abaqus™*. CRC Press. Boca Raton, FL (2013).
26. Hashin, Z. Failure Criteria for Unidirectional Fiber Composites. *Journal of Applied Mechanics*. **47** (2), 329-334 (1980).
27. Yu, W.J., Kim, H.C. Double Tapered FRP Beam for Automotive Suspension Leaf Spring. *Composite Structures*. **9**, 279-300 (1988).
28. Shokrieh, M.M., Rezaei, D. Analysis and optimization of composite leaf spring. *Composite Structures*. **60**, 317-325 (2003).
29. Wood, K. *Composite leaf springs: Saving weight in production*. <https://www.compositesworld.com/articles/composite-leaf-springs-saving-weight-in-production-suspension-systems> (2014).